2. F.C. Chen, J.M. Qiu, and Q.X. Chu, Dual-band bandstop filter using stub-loaded resonators with sharp rejection characteristic, Electron Lett 49 (2013), 351–353.
3. M.K. Mandal, K. Divyabramham, and V.K. Velidi, Compact wide-band bandstop filter with five transmission zeros, IEEE Microwave Wireless Compon Lett 22 (2012), 4–6.
4. J.I. Park, C.S. Kim, J. Kim, J.S. Park, Y. Qian, D Ahn, and T. Itoh, Modeling of a photonic bandgap and its application for the low-pass filter design, In: IEEE Asia Pacific Microwave Conference, Vol. 2, Singapore, 1999, pp. 331–334.
5. D.S. La, Y.H. Lu, and J.L. Zhang, Compact low-pass filters using novel Φ-shape defected ground structure, Microwave Opt Technol Lett 53 (2011), 1456–1459.
6. D.S. La, Y.H. Lu, S.Y. Sun, N. Liu, and J.L. Zhang, A novel compact bandstop filter using defected microstrip structure, Microwave Opt Technol Lett 53 (2011), 433–435.

SMALL-SIZE TRIPLE-WIDEBAND LTE TABLET DEVICE ANTENNA WITH A WIDEBAND FEED STRUCTURE FORMED BY INTEGRATED MATCHING NETWORK

Kin-Lu Wong and Tseng-Wei Weng
Department of Electrical Engineering, National Sun Yat-sen University, Kaohsiung 80424, Taiwan; Corresponding author: wongkl@ema.ee.nsysu.edu.tw

Received 31 March 2014

ABSTRACT: *A small-size tablet device antenna with three wide operating bands of 698–960 MHz (low band), 1710–2690 MHz (middle band), and 3400–3800 MHz (high band) for the long term evolution operation is presented. The antenna occupies a small ground clearance of 10 × 30 mm^2 and has a thin thickness of 3 mm in the tablet device such as a tablet computer in this study. The antenna comprises three radiating branches (Branch 1, Branch 2, and Branch 3) and a wideband feed structure formed by the integrated matching network. Branch 1 and 2 are connected through a series chip inductor to control the antenna's first two resonant modes to occur in the desired low band and middle band, and Branch 3 generates a resonant mode in the desired high band. The integrated matching network comprises a shunt chip capacitor, a shunt chip inductor, and a series chip capacitor to cause dual-resonance of the antenna's three resonant modes contributed by the three branches, thereby greatly enhancing the low-band, middle-band, and high-band bandwidths to cover the desired operating bands of 698–960, 1710–2690, and 3400–3800 MHz. Details of the proposed antenna are described. Operating principle of the wideband feed structure formed by the integrated matching circuit is also discussed.* © 2014 Wiley Periodicals, Inc. Microwave Opt Technol Lett 56:2507–2512, 2014; View this article online at wileyonlinelibrary.com. DOI 10.1002/mop.28624

Key words: *mobile antennas; tablet device antennas; LTE antennas; triple-wideband antennas; small-size antennas; wideband feed structure*

1. INTRODUCTION

For fourth-generation communications, the tablet mobile devices are mainly required to support the long term evolution (LTE) operation, which includes the operating bands of 698–960/1710–2170/2300–2400/2500–2690/3400–3800 MHz [1, 2]. Although there have been many LTE antennas reported recently for the smartphones [3–13], notebook computers [14–18] or tablet computers [19–26], they mainly covers two wide operating bands of 698–960 and 1710–2690 MHz only. There are very few reported antennas that can support three wide operating bands of 698–960, 1710–2690, and 3400–3800 MHz to cover the allocated LTE bands [1, 2]. In the recently reported triple-wideband tablet device antenna in [2], the antenna occupies a ground clearance of 10 × 45 mm^2 to support the desired three wide bands for the LTE operation. The antenna is easy to fabricate on an FR4 substrate [2]. However, in modern tablet devices, the ground clearance therein is becoming very limited for accommodating the embedded antenna. This makes it demanded that the occupied ground clearance of the embedded antenna therein should be as small as possible. To meet this requirement, new LTE antenna design with smaller occupied ground clearance is still an open issue and is attractive for practical applications.

In this article, we present an LTE antenna using a novel wideband feed structure to result in dual-resonance excitation of the antenna's three resonant modes generated by three radiating branches thereof. The three branches are configured into a compact structure such that the proposed antenna requires a small ground clearance of 10 × 30 mm^2 in the tablet device such as a tablet computer in this study. The occupied ground clearance is smaller than those of the dual-wideband or triple-wideband LTE antennas that have been reported recently [2–26]. In addition, the antenna has a thin thickness of 3 mm, which is promising for the modern slim tablet device application.

In the proposed design, the wideband feed structure is formed by the integrated matching network consisting of a shunt chip capacitor, a shunt chip inductor, and a series chip capacitor. With the aid of the shunt capacitor in the wideband feed structure, enhanced bandwidths of the antenna's middle band and high band can be obtained. Conversely, the shunt inductor and series capacitor effectively increase the antenna's low-band bandwidth. Hence, with the proposed wideband feed structure, the antenna can provide a triple-wideband operation to cover the LTE operation in the 698–960, 1710–2690, and 3400–3800 MHz bands. Details of the proposed antenna are described. Operating principle of the wideband feed structure in achieving the triple-wideband operation is discussed in this study, and simulated and experimental results of the proposed antenna are presented.

2. PROPOSED ANTENNA AND ITS OPERATING PRINCIPLE

Figure 1(a) shows the triple-wideband LTE antenna with a wideband feed structure for the tablet computer application. The antenna comprises a printed metal pattern and a bent metal plate. The printed metal pattern is fabricated on a 0.8-mm thick FR4 substrate of size 10 × 30 mm^2, relative permittivity 4.4, and loss tangent 0.024. Detailed dimensions of the printed metal pattern are presented in Figure 1(b). The wideband feed structure is also disposed on the FR4 substrate, and its equivalent circuit model is shown in Figure 2. The bent metal plate is cut from a 0.2-mm thick copper plate and connected to the printed metal pattern on the FR4 substrate. Note that the occupied ground clearance of the antenna is 10 × 30 mm^2 only, and the antenna's total volume is 10 × 30 × 3 mm^3 only. The antenna is mounted along the top edge of the device ground plane of a tablet computer. The ground plane is selected to have a size of 200 × 150 mm^2, which is about the size of a practical 9.7-inch tablet computer. The photos of the fabricated antenna in its front and back views are also presented in Figure 3(a) to provide a clear picture of the proposed antenna. In Figure 3(b), the antenna is mounted at the top edge of the device ground plane for experimental testing in this study.

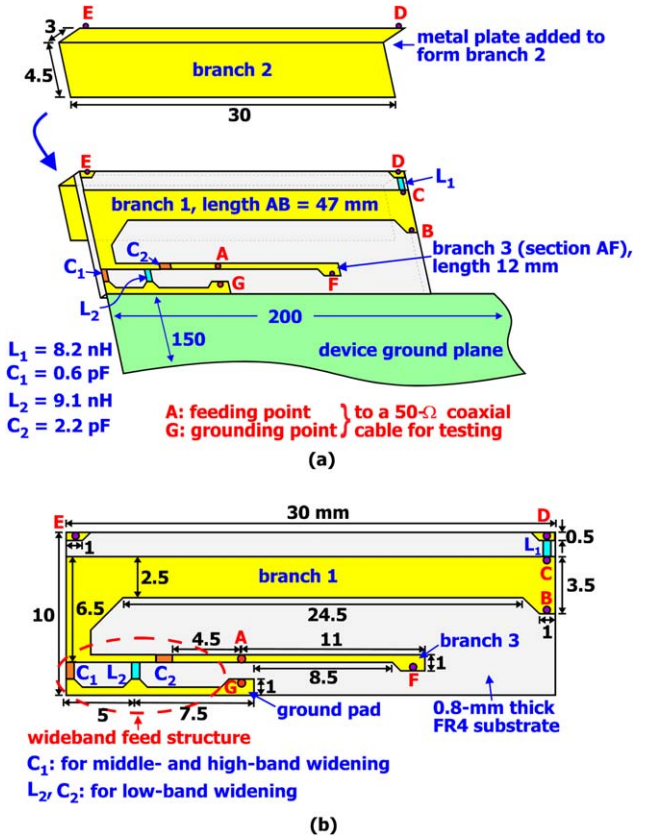

Figure 1 (a) Geometry of the triple-wideband LTE antenna with a wideband feed structure for the tablet computer application. (b) Dimensions of antenna's printed metal pattern. [Color figure can be viewed in the online issue, which is available at wileyonlinelibrary.com]

The antenna comprises three radiating branches, which are Branch 1, Branch 2, and Branch3. The three branches contribute to three resonant modes in the desired low, middle and high bands. Branch 1 (Section AB) has a length of about 47 mm, which is close to 0.25 wavelength at about 1.7 GHz and can hence generate a resonant mode in the desired middle band. Branch 2 is the bent metal plate, which is connected to point D and E to be fixed to the FR4 substrate. At point D, Branch 2 is also connected to Branch 1 through a chip inductor L_1 of 8.2 nH. Owing to the inductor L_1, Branch 2 has small effects on the

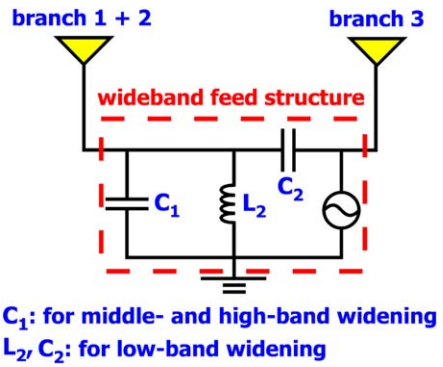

Figure 2 Equivalent circuit model of the wideband feed structure. [Color figure can be viewed in the online issue, which is available at wileyonlinelibrary.com]

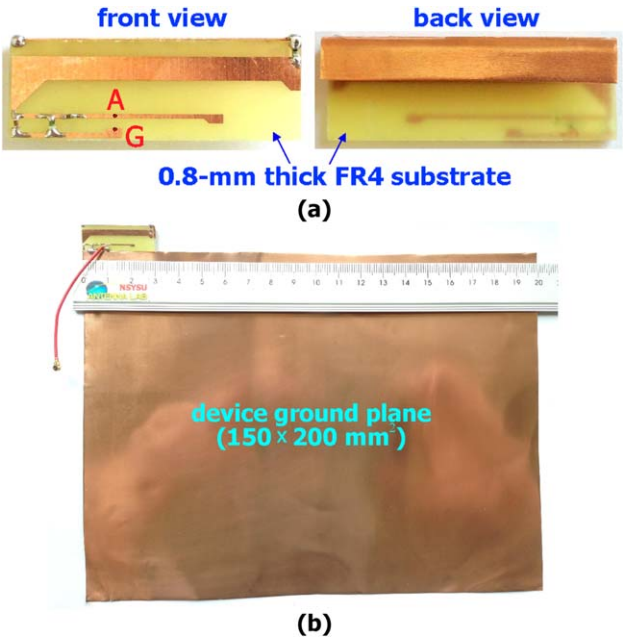

Figure 3 Photos of (a) the fabricated antenna and (b) the same mounted at the top edge of the device ground plane for experimental testing. [Color figure can be viewed in the online issue, which is available at wileyonlinelibrary.com]

generated resonant mode in the middle band controlled by Branch 1. Furthermore, the inductor L_1 contributes additional inductance at lower frequencies such that the effective resonant length provided by both Branch 1 and Branch 2 increases [27]. This leads to a resonant mode generated in the desired low band. A third resonant mode is controlled by Branch 3 (Section AF, length 12 mm) and occurs at frequencies in the desired high band. By adjusting the lengths of Branch 1, 2, and 3, the three resonant modes can be controlled. However, it is noted that the three resonant modes are with narrow bandwidths and are far from covering the desired three wide operating bands for the LTE operation.

The wideband feed structure is formed by the integrated matching network, which comprises a shunt chip capacitor C_1 (0.6 pF), a shunt chip inductor L_2 (9.1 nH), and a series chip capacitor C_2 (2.2 pF). The shunt capacitor C_1 can lead to dual-resonance for the antenna's second and third resonant modes, such that the antenna's middle- and high-band bandwidths are greatly increased to cover the desired 1710–2690 and 3400–3800 MHz bands. In addition, the shunt capacitor C_1 has small effects on the antenna's low-band performance. That is, the shunt capacitor C_1 functions like a low-pass matching circuit. Conversely, the shunt inductor L_2 and series capacitor C_2 form like a high-pass matching circuit to cause dual-resonance for the antenna's low band, with relatively small effects on the antenna's middle- and high-band performance. In this case, the antenna's low-band bandwidth can also be greatly increased to cover the desired 698–960 MHz band.

To analyze the operating principle of the antenna more clearly, Figure 4 shows the simulated return loss for the proposed antenna, the case with branch 1 only (Ant1), the case with Branch 1 and 2 only (Ant2) and the case with Branch 1, 2, and 3 only (Ant3). Corresponding dimensions of all the antennas shown in the figure are the same. Ant1, Ant2, and Ant3 in the figure are without the integrated matching network. That is,

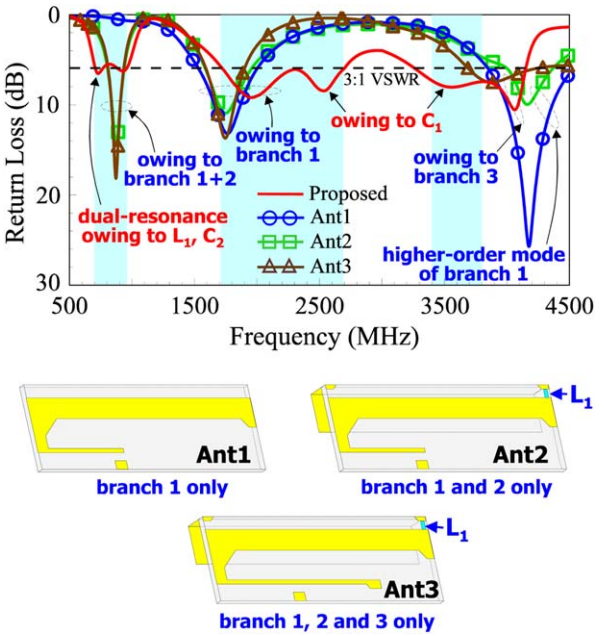

Figure 4 Simulated return loss for the proposed antenna, the case with branch 1 only (Ant1), the case with Branch 1 and 2 only (Ant2), and the case with branch 1, 2, and 3 only (Ant3). Corresponding dimensions are the same as given in Fig. 1. [Color figure can be viewed in the online issue, which is available at wileyonlinelibrary.com]

Ant1, Ant2, and Ant3 are with a simple feed structure. The simulated results are obtained using the full-wave electromagnetic field simulator HFSS version 15 [28]. The three desired bands (low, middle, and high bands) are indicated by shaded frequency regions in the figure. For Ant1, it is seen that a resonant mode owing to Branch 1 occurs in the middle band. The bandwidth of the resonant mode is seen to be far from covering the desired 1710–2690 MHz band. For Ant2, an additional resonant mode owing to Branch 1 and 2 are excited at about 0.9 GHz, with the resonant mode owing to Branch 1 alone very slightly affected. This behavior is owing to the inductor L_1 embedded between Branch 1 and 2 [27]. The frequency ratio of

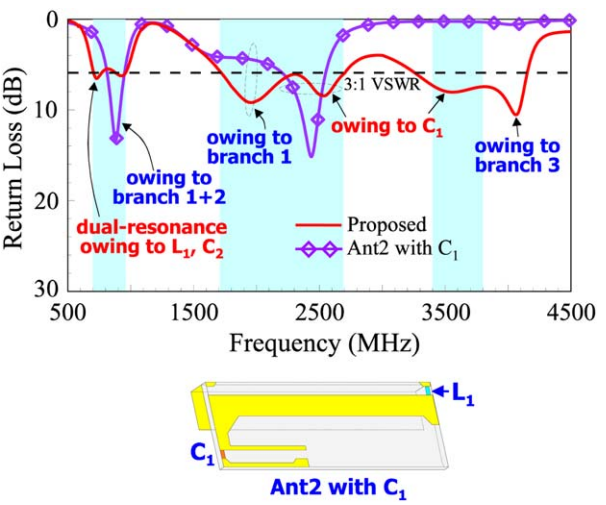

Figure 5 Simulated return loss for the proposed antenna and the case of Ant2 with the shunt capacitor C1. Corresponding dimensions are the same as given in Figure 1. [Color figure can be viewed in the online issue, which is available at wileyonlinelibrary.com]

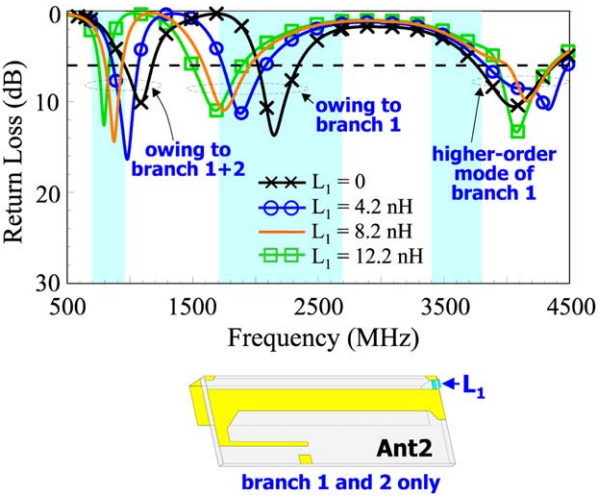

Figure 6 Simulated return loss for Ant2 as a function of the inductor L1. Other parameters are the same as given in Figure 1. [Color figure can be viewed in the online issue, which is available at wileyonlinelibrary.com]

the two resonant mode occurred in the low and middle bands can also be adjusted by the inductor L_1, which will be discussed with the aid of Figure 6 later.

For Ant3, it is seen that a resonant mode at about 4 GHz is excited, which is owing to Branch 3. By comparing Ant3 to the proposed antenna, it is seen that dual-resonance for all the three resonant modes is obtained, making the antenna have three wide operating bands for the LTE operation. Note that the dual-resonance in the low band is owing to the inductor L_2 and capacitor C_2, while the dual-resonance in the middle and high bands is owing to the capacitor C_1. In addition, it should be noted that the resonant mode occurred at about 4.2 GHz for Ant1 and Ant2 is the higher-order mode of Branch 1. This resonant mode, however, is suppressed when the capacitor C_1 is present, which is required to provide dual-resonance for the antenna's middle band. This behavior can be seen clearly in Figure 5, where the simulated return loss for the proposed antenna and the case of Ant2 with the shunt capacitor C_1 is presented. Hence, to generate a resonant mode for the antenna's high band, Branch 3 is added. It is also noted that the capacitor C_1 is properly selected such that it can cause dual-resonance for the resonant mode contributed by Branch 3 as well. Hence, with the

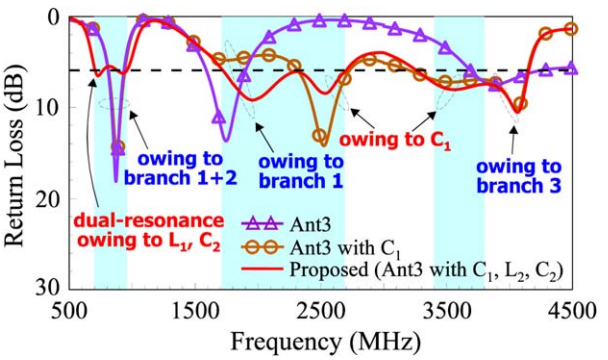

Figure 7 Simulated return loss for Ant3, Ant3 with C1 only, and Ant3 with C1, L2, and C2 (proposed design). [Color figure can be viewed in the online issue, which is available at wileyonlinelibrary.com]

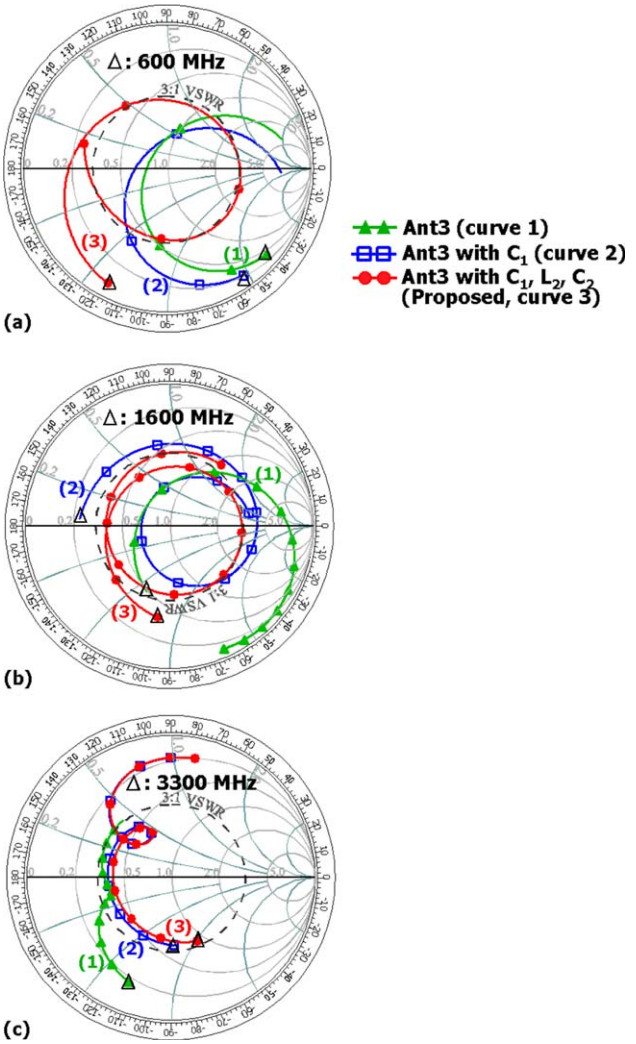

Figure 8 Simulated input impedance on the Smith chart for Ant3 (Curve 1), Ant3 with C1 only (Curve 2), and Ant3 with C1, L2, C2 (Curve 3, proposed design). (a) Frequency range from 600 to 1000 MHz. (b) Frequency range from 1600 to 2800 MHz. (c) Frequency range from 3300 to 4500 MHz. [Color figure can be viewed in the online issue, which is available at wileyonlinelibrary.com]

presence of the wideband feed structure, the proposed antenna can provide a triple-wideband operation covering the desired 698–960, 1710–2690, and 3400–3800 MHz bands (see results of the proposed antenna vs. Ant3 in Fig. 4). Also note that although the impedance matching for some frequencies in the low band is slightly less than 6 dB (3:1 VSWR), the antenna efficiency including the mismatching loss is better than about 60%, which is good for practical mobile communication applications [2, 29, 30].

To show the antenna's first two resonant modes owing to Branch 1 and 2 as a function of the inductor L_1, the simulated return loss for L_1 varied from 0 to 12.2 nH is presented in Figure 6. For $L_1 = 0$, it indicates that Branch 2 is directly connected to Branch 1. Results show that by selecting a proper inductance of L_1 (see the results for 8.2 nH in the figure), the first two resonant modes can be controlled to occur in the antenna's low band and middle band, respectively. In the proposed design, L_1 is hence selected to be 8.2 nH.

Detailed effects of the integrated matching network in the wideband feed structure are analyzed with the aid of Figures 7 and 8. In Figure 7, the simulated return loss for Ant3, Ant3 with C_1 only, and Ant3 with C_1, L_2, and C_2 (proposed design) is presented. When the capacitor C_1 is added to Ant3, dual-resonance in the antenna's middle and high bands is seen. When the inductor L_2 and capacitor C_2 is further added, dual-resonance in the antenna's low band is seen. The impedance matching for frequencies in the lower region of the middle band is also improved. Very small effects on the antenna's high-band performance are seen. From the results, it can be concluded that the inductor L_2 and capacitor C_2 function like a high-pass matching circuit, while the capacitor C_1 functions like a low-pass matching circuit.

The simulated input impedance on the Smith chart for Ant3 (Curve 1), Ant3 with C_1 only (Curve 2), and Ant3 with C_1, L_2, and C_2 (Curve 3, proposed design) is also presented in Figure 8. Results for the frequency range from 600 to 1000 MHz are shown in Figure 8(a). Those for the frequency ranges from 1600 to 2800 MHz and from 3300 to 4500 MHz are shown in Figures 8(b) and 8(c), respectively. In Figure 8(a), small effects on the impedance matching are seen when the capacitor C_1 is added (see Curve 1 vs. Curve 2). Conversely, a loop curve indicating dual-resonance occurred is seen when the inductor L_2 and capacitor C_2 is further added (see Curve 2 vs. Curve 3).

In Figure 8(b) for the middle band, when the capacitor C_1 is added, the impedance curve is shifted into a loop curve showing that dual-resonance occurs (see Curve 1 vs. Curve 2). When the inductor L_2 and capacitor C_2 is further added, the loop curve is still present, with impedance matching further improved (see Curve 2 vs. Curve 3). In Figure 8(c) for the high band, very small variations between Curve 2 and 3 are seen. This confirms that the inductor L_2 and capacitor C_2 function like a high-pass matching circuit. Conversely, the capacitor C_1 causes dual-resonance (see Curve 1 vs. Curve 2) for the impedance curve in

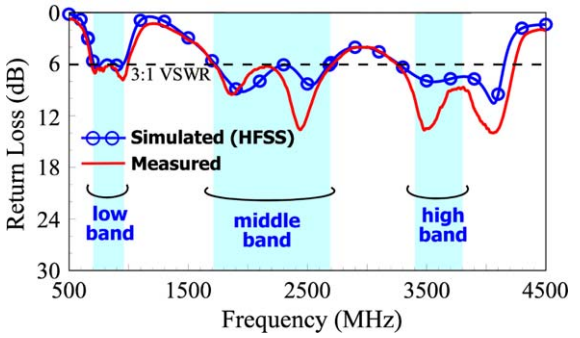

Figure 9 Measured and simulated return loss of the fabricated antenna. [Color figure can be viewed in the online issue, which is available at wileyonlinelibrary.com]

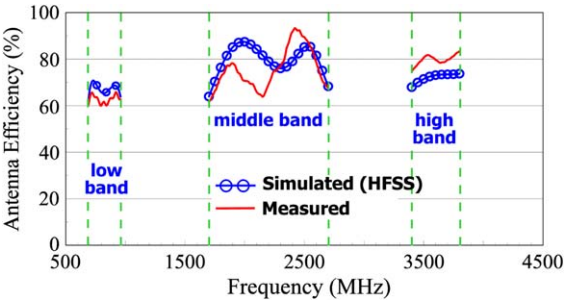

Figure 10 Measured and simulated antenna efficiency of the fabricated antenna. [Color figure can be viewed in the online issue, which is available at wileyonlinelibrary.com]

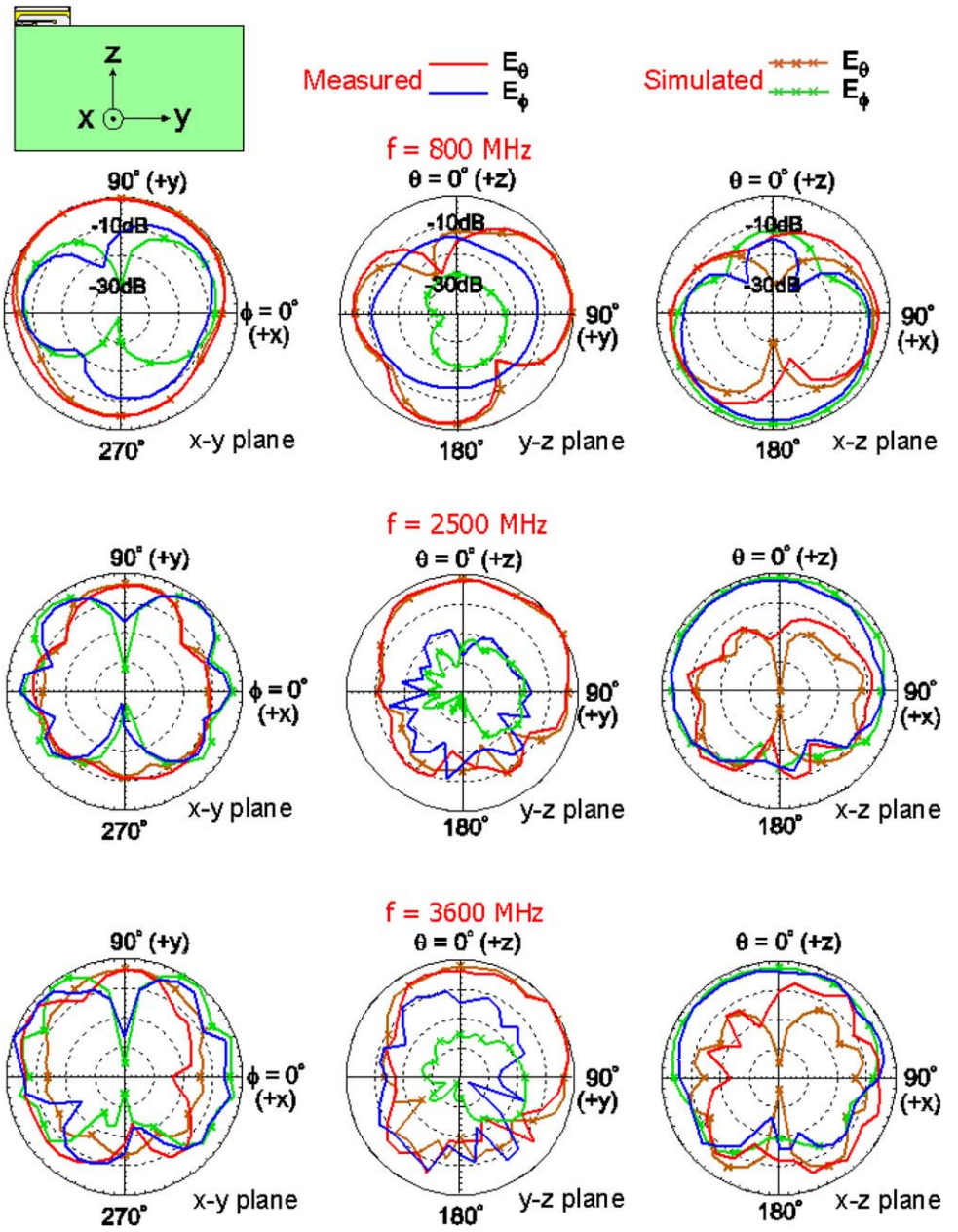

Figure 11 Measured radiation patterns of the fabricated antenna at 800, 2500, and 3600 MHz. [Color figure can be viewed in the online issue, which is available at wileyonlinelibrary.com]

the antenna's high band. The results confirm that the wideband feed structure with the elements C_1, L_2, and C_2 can lead to a triple-wideband operation for the antenna.

3. EXPERIMENTAL RESULTS

Figure 9 shows the measured and simulated return loss of the fabricated antenna (see the photos in Fig. 3). A 50-Ω coaxial line is connected to point A and G (see Fig. 1) for the experimental testing. Agreement between the simulated results and measured data is seen. The antenna shows a triple-wideband operation covering the 698–960, 1710–2690, and 3400–3800 MHz for the LTE operation. Results of the measured and simulated antenna efficiency are presented in Figure 10. The antenna's radiation performance is measured in a far-field anechoic chamber. The antenna efficiency includes the mismatching loss. The measured antenna efficiency reaches about 60–66%, 62–92%, and 75–82% for frequencies in the low, middle, and high bands, respectively. The results are acceptable for mobile communication applications [2, 29, 30]. Note that the measured antenna efficiency generally agree with the simulated results. For frequencies in the high band, the measured antenna efficiency is larger than the simulated results, which may be owing to the measured return loss being better than the simulated return loss. Therefore, it is reasonable that better antenna efficiency in the measurement is obtained.

Figure 11 shows the measured radiation patterns of the fabricated antenna at 800, 2500, and 3600 MHz. At each frequency, results in three principal planes are presented. The radiation

intensities in the three planes are normalized with respect to the same maximum intensity. The measured radiation patterns are seen to be in agreement with the simulated results. In the azimuthal plane (x-y plane), near-omnidirectional radiation is seen at 800 MHz, while comparable E_θ and E_ϕ radiation is seen at 2500 and 3600 MHz. In the elevation planes (x-z and y-z planes), stronger radiation is seen in the lower half-plane in the $-z$ direction at 800 MHz, while stronger radiation is seen in the upper half-plane in the $+z$ direction at 2500 and 3600 MHz. This suggests that the device ground plane also contributes to the radiation in the antenna's low band. However, in the antenna's middle and high bands, the device ground plane functions more like as a reflector. The radiation characteristics are similar to those observed for the triple-wideband LTE antenna reported in [2].

4. CONCLUSION

A triple-wideband LTE antenna with a small occupied ground clearance of 10×30 mm^2 and a thin thickness of 3 mm in the tablet computer has been proposed. The triple-wideband operation in the desired low band (698–960 MHz), middle band (1710–2690 MHz), and high band (3400–3800 MHz) is achieved by embedding a wideband feed structure to the antenna. Operating principle of the wideband feed structure has been discussed. Good radiation characteristics for frequencies in the three wide operating bands have also been observed. The proposed antenna is promising for practical applications in modern slim tablet computers.

REFERENCES

1. LTE Frequency Bands & Spectrum Allocations-a summary: tables of the LTE frequency band spectrum allocations for 3G & 4G LTE—TDD and FDD. Available at: http://www.radio-electronics.com/.
2. K.L. Wong and T.W. Weng, Small-size triple-wideband LTE/WWAN tablet device antenna, IEEE Antennas Wireless Propag Lett 12 (2013), 1516–1519.
3. F.H. Chu and K.L. Wong, Simple planar printed strip monopole with a closely-coupled parasitic shorted strip for eight-band LTE/GSM/UMTS mobile phone, IEEE Trans Antennas Propag 58 (2010), 3426–3431.
4. C.T. Lee and K.L. Wong, Planar monopole with a coupling feed and an inductive shorting strip for LTE/GSM/UMTS operation in the mobile phone, IEEE Trans Antennas Propag 58 (2010), 2479–2483.
5. C.W. Chiu, C.H. Chang, and Y.J. Chi, A meandered loop antenna for LTE/WWAN operations in a smartphone, Prog Electromagn Res C 16 (2010), 147–160.
6. K.L. Wong and W.Y. Chen, Small-size printed loop-type antenna integrated with two stacked coupled-fed shorted strip monopoles for eight-band LTE/GSM/UMTS operation in the mobile phone, Microwave Opt Technol Lett 52 (2010), 1471–1476.
7. F.H. Chu and K.L. Wong, On-board small-size printed LTE/WWAN mobile handset antenna closely integrated with nearby system ground plane, Microwave Opt Technol Lett 53 (2011), 1336–1343.
8. F.H. Chu and K.L. Wong, Internal coupled-fed dual-loop antenna integrated with a USB connector for WWAN/LTE mobile handset, IEEE Trans Antennas Propag 59 (2011), 4215–4221.
9. K.L. Wong, T.W. Kang, and M.F. Tu, Internal mobile phone antenna array for LTE/WWAN and LTE MIMO operations, Microwave Opt Technol Lett 53 (2011), 1569–1573.
10. S. Jeon and H. Kim, Mobile terminal antenna using a planar inverted-E feed structure for enhanced impedance bandwidth, Microwave Opt Technol Lett 54 (2012), 2133–2138.
11. Y.L. Ban, C.L. Liu, J.L.W. Li, J. Guo, and Y. Kang, Small-size coupled-fed antenna with two printed distributed inductors for seven-band wwan/lte mobile handset, IEEE Trans Antennas Propag 61 (2013), 5780–5784.
12. C.Y.D. Sim and Y.L. Chien, A dual-band coupled-fed LTE/WWAN planar antenna for mobile devices, Microwave Opt Technol Lett 55 (2013), 1851–1856.
13. R. Valkonen, M. Kaltiokallio, and C. Icheln, Capacitive coupling element antennas for multi-standard mobile handsets, IEEE Trans Antennas Propag 61 (2013), 2783–2791.
14. D.L. Huang, H.L. Kuo, C.F. Yang, C.L. Liao, and S.T. Lin, Compact multibranch inverted-F antenna to be embedded in a laptop computer for LTE/WWAN/IMT-E Applications, IEEE Antennas Wireless Propag Lett 9 (2010), 838–841.
15. C.L. Ku, W.F. Lee, and S.T. Lin, A compact slot inverted-F antenna to be embedded in the laptop computer for LTE/WWAN applications, Microwave Opt Technol Lett 53 (2011), 1829–1832.
16. T.W. Kang, K.L. Wong, L.C. Chou, and M.R. Hsu, Coupled-fed shorted monopole with a radiating feed structure for eight-band LTE/WWAN operation in the laptop computer, IEEE Trans Antennas Propag 59 (2011), 674–679.
17. C.L. Ku, W.F. Lee, and S.T. Lin, A compact slot inverted-F antenna to be embedded in the laptop computer for LTE/WWAN applications, Microwave Opt Technol Lett 53 (2011), 1829–1832.
18. Y.L. Ban, S.C. Sun, J.L.W. Li, and W. Hu, Compact coupled-fed wideband antenna for internal eight-band LTE/WWAN tablet computer applications, J Electromagn Waves Appl 26 (2012), 2222–2233.
19. S.H. Chang and W.J. Liao, A broadband LTE/WWAN antenna design for tablet PC, IEEE Trans Antennas Propag 60 (2012), 4354–4359.
20. K.L. Wong and T.J. Wu, Small-size LTE/WWAN coupled-fed loop antenna with band-stop matching circuit for tablet computer, Microwave Opt Technol Lett 54 (2012), 1189–1193.
21. J.H. Lu and Y.S. Wang, Internal uniplanar antenna for LTE/GSM/UMTS operation in a tablet computer, IEEE Trans Antennas Propag 61 (2013), 2841–2846.
22. W.S. Chen and W.C. Jhang, A planar WWAN/LTE antenna for portable devices, IEEE Antennas Wireless Propag Lett 12 (2013), 19–23.
23. K.L. Wong, H.J. Jiang, and T.W. Weng, Small-size planar LTE/WWAN antenna and antenna array formed by the same for tablet computer application, Microwave Opt Technol Lett 55 (2013), 1928–1934.
24. K.L. Wong and M.T. Chen, Small-size LTE/WWAN printed loop antenna with an inductively coupled branch strip for bandwidth enhancement in the tablet computer, IEEE Trans Antennas Propag 61 (2013), 6144–6151.
25. K.L. Wong and L.Y. Chen, Coupled-fed inverted-F antenna using an inverted-F coupling feed for small-size LTE/WWAN tablet computer antenna, Microwave Opt Technol Lett 56 (2014), 1296–1302.
26. K.L. Wong and T.W. Weng, Coupled-fed shorted strip antenna with an inductively coupled branch strip for low-profile, small-size LTE/WWAN tablet computer antenna, Microwave Opt Technol Lett 56 (2014), 1041–1046.
27. K.L. Wong and S.C. Chen, Printed single-strip monopole using a chip inductor for penta-band WWAN operation in the mobile phone, IEEE Trans Antennas Propag 58 (2010), 1011–1014.
28. ANSYS HFSS. Available at: http://www.ansys.com/products/hf/hfss/.
29. K.L. Wong, Y.W. Chang, and S.C. Chen, Bandwidth enhancement of small-size WWAN tablet computer antenna using a parallel-resonant spiral slit, IEEE Trans Antennas Propag 60 (2012), 1705–1711.
30. K.L. Wong, T.J. Wu, and P.W. Lin, Small-size uniplanar WWAN tablet computer antenna using a parallel-resonant strip for bandwidth enhancement, IEEE Trans Antennas Propag 61 (2013), 492–496.